Is protein deuteration beneficial for proton detected solid-state NMR at and above 100 kHz magic-angle spinning?

Diane Cala - de Paepe, Jan Stanek, Kristaps Jaudzems, Kaspars Tars, Loren
B Andreas, Guido Pintacuda

HAL Id: hal-01575517

https://hal.science/hal-01575517

Submitted on 15 Mar 2018

Is protein deuteration beneficial for proton detected solid-state NMR at and above 100 kHz magic-angle spinning?

Diane Cala-De Paepe,[a*] Jan Stanek,[a*] Kristaps Jaudzems,[a] Kaspars Tars,[b] Loren B Andreas,[a,c] Guido Pintacuda[a#]

[a] Centre de RMN à Très Hauts Champs, Institut des Sciences Analytiques (UMR 5280 – CNRS, ENS Lyon, UCB Lyon 1), Université de Lyon, 5 rue de la Doua, 69100 Villeurbanne, France
[b] Biomedical Research and Study Centre, Rātsupītes 1, LV1067, Riga, Latvia
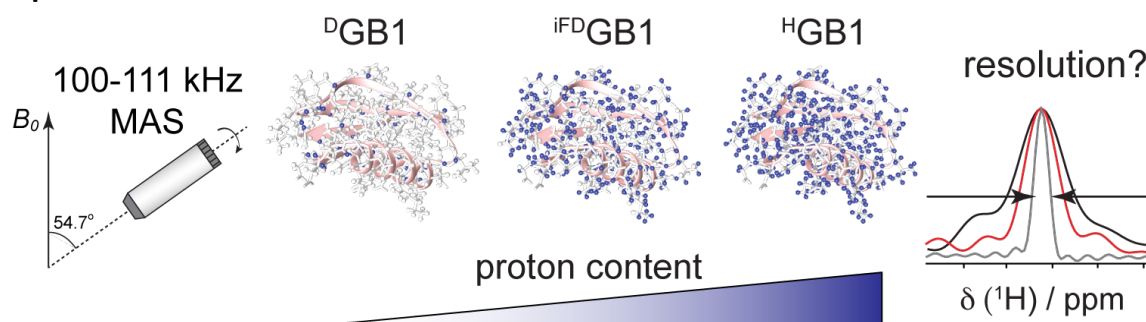[c] Max Planck Institute for Biophysical Chemistry, Am Fassberg 11, D-37077 Göttingen, Germany

* These authors contributed equally
# Corresponding author: guido.pintacuda@ens-lyon.fr (Guido Pintacuda)

Abstract

^{1}H-detection in solid-state NMR of proteins has been traditionally combined with deuteration for both resolution and sensitivity reasons, with the optimal level of proton dilution being dependent on MAS rate. Here we present [1]H-detected ^{15}N and ^{13}C CP-HSQC spectra on two microcrystalline samples acquired at 60 and 111 kHz MAS and at ultra-high field. We critically compare the benefits of three labeling schemes yielding different levels of proton content in terms of resolution, coherence lifetimes and feasibility of scalar-based 2D correlations under these experimental conditions. We observe unexpectedly high resolution and sensitivity of aromatic resonances in 2D [13]C-^{1}H correlation spectra of protonated samples. Ultrafast MAS reduces or even removes the necessity of ^{1}H dilution for high-resolution [1]H-detection in biomolecular solid-state NMR. It yields ^{15}N,[1]H and ^{13}C,[1]H fingerprint spectra of exceptional resolution for fully protonated samples, with notably superior ^{1}H and ^{13}C lineshapes for side-chain resonances.

Graphical Abstract

Highlights

- Fast MAS weakens ^{1}H dilution requirements for [1]H-detection in biomolecular ssNMR
- The ^{1}H resolution enhancement due to deuteration drops with increasing MAS rate
- Proton coherence lifetime remains strongly dependent on deuteration level
- Fractional deuteration yields limited linewidth improvement at above 100 kHz MAS
- Fully-protonated samples provide optimal ^{1}H and ^{13}C resolution for methyl resonances

Keywords

Fast magic-angle spinning, proton detection, proteins, protein assemblies, full protonation, resolution, sensitivity, side-chains, fractional deuteration, solid-state nuclear magnetic resonance

Abbreviations

[D]**GB1** = [U-^{2}H,U-^{13}C,U-^{15}N]-GB1, uniformly ^{2}H,[13]C,[15]N-labelled immunoglobulin-binding beta 1 domain of protein G (GB1), with 100% [1]H at exchangeable sites

[iFD]**GB1** = inverse fractionally deuterated GB1, [^{2}H/^{1}H,U-^{13}C,U-^{15}N]-GB1, expressed in H_2O growth medium with deuterated glucose as a sole carbon source

[H]**GB1** = [U-^{13}C,U-^{15}N]-GB1, fully protonated, uniformly ^{13}C,[15]N-labelled GB1

[iFD]**AP205** = inverse fractionally deuterated AP205, [^{2}H/^{1}H,U-^{13}C,U-^{15}N]-AP205, expressed in H_2O growth medium deuterated glucose as a sole carbon source

[H]**AP205** = [U-^{13}C,U-^{15}N]-AP205, fully protonated, uniformly ^{13}C,[15]N-labelled *Acinetobacter phage* 205 coat protein

1. Introduction

Proton detection is the most natural way to maximize sensitivity in NMR [1, 2]. Protons not only have high gyromagnetic ratio, but are also abundant in biomolecules. In solids, however, this generates a dense network of homonuclear dipolar interactions, which induces significant ^{1}H line broadening at moderate magic-angle spinning (MAS), and makes ^{1}H lines prohibitive for constructive use [3].

To tackle this difficultly, MAS was originally combined with an extreme dilution of the proton content in the sample [4-6]. For most proteins, a high level of deuteration can be achieved by expression in perdeuterated media, followed by a chemical exchange of labile deuterons with protons of the solvent with a desired H_2O/D_2O ratio. In the pioneering studies of Zilm and Reif, amide ^{1}H were fully reintroduced leading to a moderate resolution improvement [7, 8]. It was soon demonstrated, however, that at 10-20 kHz MAS feasible a decade ago, higher resolution is obtained by further dilution at amide ^{1}H sites (typically 10-40%) [9]. The optimum deuteration level was a trade-off between higher resolution and detection sensitivity, as increased dilution results in a loss of signal of the observed nuclei [10, 11].

This issue has driven the development of probes capable of faster MAS, which have been increasingly more effective in averaging ^{1}H dipolar interactions [12]. Equally important is the use of very high magnetic fields which help to separate heavily overlapped resonance frequencies of interacting protons, thus reducing ^{1}H relaxation driven by spin flip-flops [13, 14]. With these hardware advancements, the proton dilution requirements have become less stringent for NMR studies at high resolution [15-17]. In particular, it was shown that sensitive cross-polarization (CP) HSQC spectra with [1]H^N linewidths smaller than 100 Hz can be obtained for microcrystalline uniformly [^{2}H,^{13}C,^{15}N]-labeled protein samples fully back-exchanged at amide sites, under conditions of 60 kHz MAS on a 1 GHz spectrometer. Despite substantial reduction of sample amount (to 2-3 mg for a 1.3 mm) this approach yields very high sensitivity due to multiple factors as reviewed recently [13]. With the advent of even faster MAS rates in smaller rotors, larger sensitivity gains per sample volume have been reported (less than 1 mg is required for 0.8 mm [18, 19] and 0.7 mm [20] rotors).

However, chemical exchange of labile deuterons with protons severely limits observation of side-chain signals, which are essential reporters of structure, dynamics and interactions in a protein. In contrast to amide sites, introduction of protons or deuterons in side-chains can only take place during protein expression. It was first realized by the group of Reif that ^{2}H-glucose used for expression is not completely [1]H-depleted, leading to observable signal in side-chains [6, 21]. Proton occupancy at methyl sites was then increased by expression in 1:9 $H_2O:D_2O$ media using a partially protonated methyl-containing residue precursor, and high resolution ^{1}H,^{13}C-methyl correlation spectra were obtained using relaxation-filtration of isotopomers [22].

This approach was later generalized to all side-chain sites by the use of ^{2}H,^{13}C-glucose and controlled low concentration of H_2O in D_2O buffer (5-15%). This labeling scheme, termed Reduced Adjoining Protonation (RAP) [23, 24], leads to a random mixture of isotopomers, however, the problem is not severe due to high imbalance of their population at low level of ^{1}H incorporation. At 20 kHz MAS this method yielded aliphatic ^{1}H linewidths between 25 and 60 Hz for microcrystalline chicken alpha spectrin SH3 domain and enabled observation of some long-range [1]H-^{1}H distance restraints [23], however, dilution of ^{1}H spins inherently decreased the probability of such contacts. Slightly higher proton content (usually 10-40%) is achieved with so-called fractional deuteration (FD), which employs protonated glucose for expression in D_2O media [25], while high resolution is ensured by significantly faster spinning (about 55 kHz).

The proton dilution remained a major concern, since it partially offset advantages of higher sensitivity of [1]H-detection. As possible remedy is *E. coli* protein expression with the addition of suitable metabolic precursors of I, L, V residues, developed originally for liquid-state NMR [26, 27]. This provides detached protons in methyl groups, either CH_3 or CHD_2, with the possibility of reduced spectral crowding by stereo- and regiospecific labeling [28]. Despite

lower occupancy, CHD$_2$-labelling proved more useful at about 50-60 kHz MAS due to higher resolution and ease of obtaining ^{1}H-^{1}H distance restrains without dipolar truncation [18, 29]. Recently, it has been shown that under these MAS conditions, 2-fold higher sensitivity in fingerprint ^{13}C,^{1}H-correlation spectra is obtained using CH$_3$-labelling of either Ile or Ala residues. It entails certain loss of resolution but is generally advantageous in the cases of critically low sensitivity [30].

For the majority of globular proteins, methyl protons provide tertiary contacts essential to define a protein fold with high precision [29, 31]. An alternative concept that ensures 100% site incorporation and scarcity of protons is Stereo-Array Isotope Labeling (SAIL) [32]. It offers access to all side-chain sites and considerably reduces spectral crowding due flexibility and precise control over sites of incorporation with inherent absence of scrambling. With moderate MAS rate of 27 kHz, 2- to 7-fold reduction of ^{1}H linewidths was observed for valine residues [33]. Due to high cost of specifically labeled amino acids, the approach necessitates the use of cell-free expression, and has not been so far widely applied. Recently, a miniaturization of MAS rotors has partly addressed this issue allowing backbone and side-chain assignment using sub-milligram quantity of SAIL-labelled protein [34].

It is also possible to incorporate specific fully protonated amino acid residues (such as valine and leucine) into otherwise deuterated matrix, the scrambling of amino acids being dependent on biosynthetic pathways in a given expression system. The concept, referred to as proton-cloud labeling [35], has been utilized to reduce ^{1}H linewidths by a factor of 2 to 3 w.r.t. a fully protonated microcrystalline sample of ubiquitin at 60 kHz MAS.

Except SAIL, all methods described above lean on expression in highly concentrated D$_2$O, which reduces the protein yield in bacteria and is incompatible with certain expression systems, e.g. mammalian cells. Additionally, complete back-exchange of amide ^{1}H can require transient or chemically induced unfolding and refolding, which poses a particular challenge for proteins folded in the presence of suitable chaperons, or for solvent-protected sites of viral coat proteins [36] or integral membrane proteins [37, 38]. Inverse fractional deuteration (iFD) recently proposed by Medeiros-Silva and coworkers addresses this problem by expression in H$_2$O and addition of ^{2}H-glucose [39]. Despite a rather moderate level of incorporation of deuterium (10-40%, inversely to the case of FD), remarkable resolution enhancement was observed at 60 kHz MAS for ubiquitin and the ion channel KcsA. Most importantly, iFD provided access to backbone and side-chain resonances in transmembrane regions of KcsA.

Fully protonated samples are by far the easiest and least expensive to obtain. The potential of side-chain resonances for structure determination was recognized by the groups of Rienstra [40], Pintacuda [41] and Linser [42], however, detailed studies were hampered by limited resolution in ^{1}H side-chains at 40-60 kHz MAS. Recent development of probes capable of rotor spinning up to 111 kHz has dramatically improved ^{1}H resolution in fully protonated natural abundance materials and isotopically enriched biosolids [34, 43-45]. We have recently demonstrated that this new MAS condition increases the ^{1}H resolution for general application to challenging targets, in particular for atomic level structure determination of relatively large proteins [36, 46].

In this context, a series of questions become pertinent: at the magnetic field and MAS rates available today, is the highest resolution still enabled by deuteration? What is the effect of proton dilution at the highest MAS, and which labeling schemes optimize information available from backbone and side-chains? In the following, we address these questions by presenting ^{1}H-detected ^{15}N- and ^{13}C-CP-HSQC spectra for three labeling schemes yielding different levels of proton content, and we critically compare the benefits of 111 kHz and 1 GHz magnetic field in terms of resolution and coherence lifetimes on two microcrystalline samples.

2. Results and Discussion

The microcrystalline protein GB1 was used as a model system to quantify the impact of deuteration on proton resolution in ^{1}H-detected solid-state NMR spectra. Three uniformly-

[^{13}C,^{15}N]-labelled samples containing different amounts of protons were prepared: 1) a perdeuterated protein expressed in D$_2$O growth medium with deuterated glucose, with exchangeable amide ^{1}H reintroduced from protonated buffer during the purification (^{D}GB1); 2) a protein partially deuterated in side-chains expressed in H$_2$O using deuterated glucose, a. k. a. inverse fractionally deuterated [39] (^{iFD}GB1) and 3) a fully protonated protein expressed in H$_2$O with protonated glucose (^{H}GB1).

All samples were purified and crystallized according to the same protocol (see *Materials and Methods*), and packed into 0.7 mm rotors. To ensure consistent results, all NMR experiments were performed using the same MAS probe and B_0 field (25.4 T), at the same temperature, and with B_0 homogeneity monitored before every measurement. Three 2D fingerprint cross-polarization HSQC (CP-HSQC) spectra were acquired with extensive sampling in the indirect dimension for each sample: ^{15}N,^{1}H-CP-HSQC, aliphatic and aromatic ^{13}C,^{1}H-CP-HSQC. Fingerprint spectra were checked to ensure that only crystal form A of GB1 is present [47], and crystal quality was monitored on ^{15}N linewidths. A limited variability of ^{15}N shifts is observed for specific exposed residues in all preparations, which is inherent to instantaneous crystallization methods. Measurements were performed at 111 and 60 kHz MAS, thus representing the highest MAS rate available in a commercial probe (0.7 mm) and experimental conditions characteristic of the previous generation probes (1.3 mm).

Figure 1 shows a comparison of the ^{15}N-CP-HSQC spectra for the three samples and the two MAS conditions, and the representative ^{1}H cross-sections and linewidths for all resolved peaks are reported in Figure 2. The best amide ^{1}H resolution of approximately 80 Hz is achieved for ^{D}GB1 at 111 kHz (Fig. 2d), and is nearly as good at 60 kHz MAS (Fig. 2c). The resolution limit is highly specific to the sample conditions, including the target protein itself, and determined primarily by intrinsic heterogeneity (local static disorder) and, to a smaller extent, by B_0 field inhomogeneity. In this respect, GB1 spectral resolution is inferior to proteins such as chicken α-spectrin SH3 domain (best ^{1}H^N linewidths of 39±10 Hz at 23.5 T and 60 kHz MAS [15] or 19±3 Hz at 9.4 T and 24 kHz MAS [11] reported for samples in 1:9 H$_2$O:D$_2$O buffer) or ubiquitin (41±12 Hz at 20.0 T and 100 kHz MAS for a sample in 100% H$_2$O [18]) which form more ideal microcrystals. On the other hand, this larger heterogeneity brings GB1 somewhat closer to samples of particular interest of ssNMR such as protein assemblies, membrane-embedded proteins, or amyloid fibrils.

At 60 kHz MAS, full protonation (^{H}GB1) results in severe ^{1}H line broadening as the ^{1}H^N median linewidth is 247 Hz. In this spinning condition, iFD indeed represents an efficient strategy to lower the proton linewidth [39]. Here we observe a reduction of approx. 25 % with respect to ^{H}GB1, with a median linewidth of 187 Hz.

The situation is dramatically changed with increased MAS rates. The effect of changing MAS rates from 60 to 111 kHz is a 44% and 53% reduction of ^{1}H^N linewidth for ^{iFD}GB1 and ^{H}GB1, respectively, while the ^{1}H linewidth is only marginally different in ^{D}GB1. As a result, the impact of partial deuteration is far less pronounced at 111 kHz, and the ^{15}N-CP-HSQC spectra of ^{iFD}GB1 and ^{H}GB1 can hardly be distinguished (Fig. 1e,f). We estimate the overall linewidth improvement to be only 10% w.r.t. a fully protonated sample.

While only signals from amide ^{1}H can be acquired from ^{D}GB1, the two samples expressed in H$_2$O show full protonation at alpha positions, which can be monitored with ^{13}C-CP-HSQC. The excellent resolution of the α-region of the ^{13}C,^{1}H-CP HSQC enabled quantification of ^{1}Hα linewidths for 60 and 111 kHz MAS. As can be appreciated from spectra in Figure 3a-d and from representative cross-sections in Figure 4a-b, iFD considerably improves resolution at 60 kHz MAS (by approx. 25%). However, similarly to amide ^{1}H, narrower linewidths are obtained by faster spinning than by partial proton dilution. At 111 kHz, iFD undoubtedly reduces observed linewidths for all resolved resonances, but rarely more than by 20%.

Coherence lifetimes measured for ^{1}H at 60 and 111 kHz MAS provide a deeper insight into observed linewidths (Fig. 5). Most strikingly, ^{1}H^N T$_2$' increases steeply with MAS rate in this spinning regime regardless of the labeling scheme, halving the coherent contribution to the linewidths.

In the case of ^{D}GB1, ^{1}H^N coherence lifetimes of 23 ms were obtained at 111 kHz MAS. In the past literature, such long ^{1}H^N lifetimes were only reported at slower MAS rates thanks to
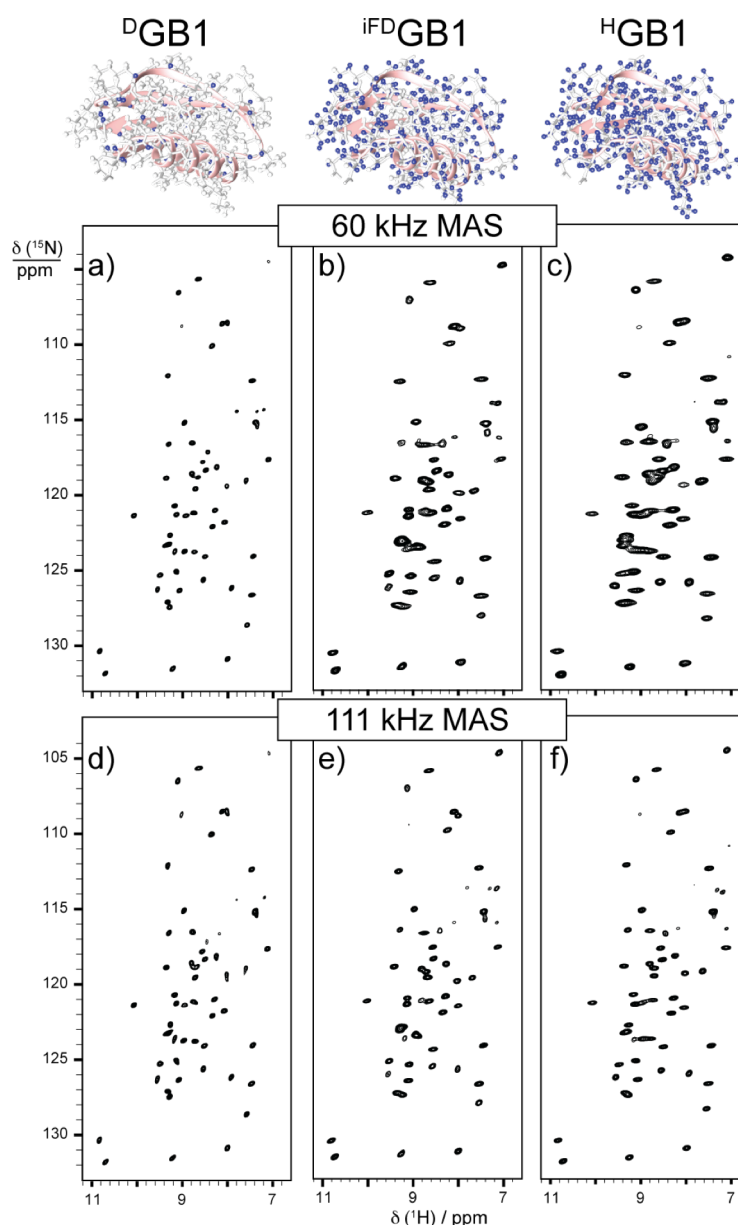
5

Fig. 1. ^{15}N-CP-HSQC of [D]GB1 (a,d), [iFD]GB1 (b,e) and [H]GB1 (c,f) recorded on a 1 GHz NMR spectrometer with 60 kHz (a,b,c) and 111 kHz MAS (d,e,f). In order to faithfully reproduce the linewidths in 2D contour plots, the lowest contour was normalized for each spectrum with respect to an average intensity of five resolved peaks (N8, T11, A26, D40, W43). The ratio of contour levels was set to 1.2.

extremely high proton dilution by perdeuteration and sparse reprotonation of exchangeable sites in D_2O/H_2O mixtures [9, 11, 15]. The improvement in coherence lifetimes due to increased MAS frequency corresponds to a decrease of the $^1H^N$ homogenous linewidth from 25 to 14 Hz (cf. Table 1), which is small compared with inhomogeneous contributions to the line, and accounts for a very minor resolution gain as observed in the ^{15}N-CP-HSQC spectra in Figure 1a,d.

In the case of the samples with higher proton content, $^1H^N T_2'$ are significantly shorter. At both spinning rates, inverse fractional deuteration increases $^1H^N$ coherence lifetime by about 40% compared to full protonation. Comparing 111 with 60 kHz MAS, the improvement in $^1H^N T_2'$ corresponds to a decrease of the $^1H^N$ homogenous linewidth from 132 to 46 Hz, and from 182 to 59 Hz, for $^{iFD}GB1$ and $^HGB1$, respectively. These values represent a substantial

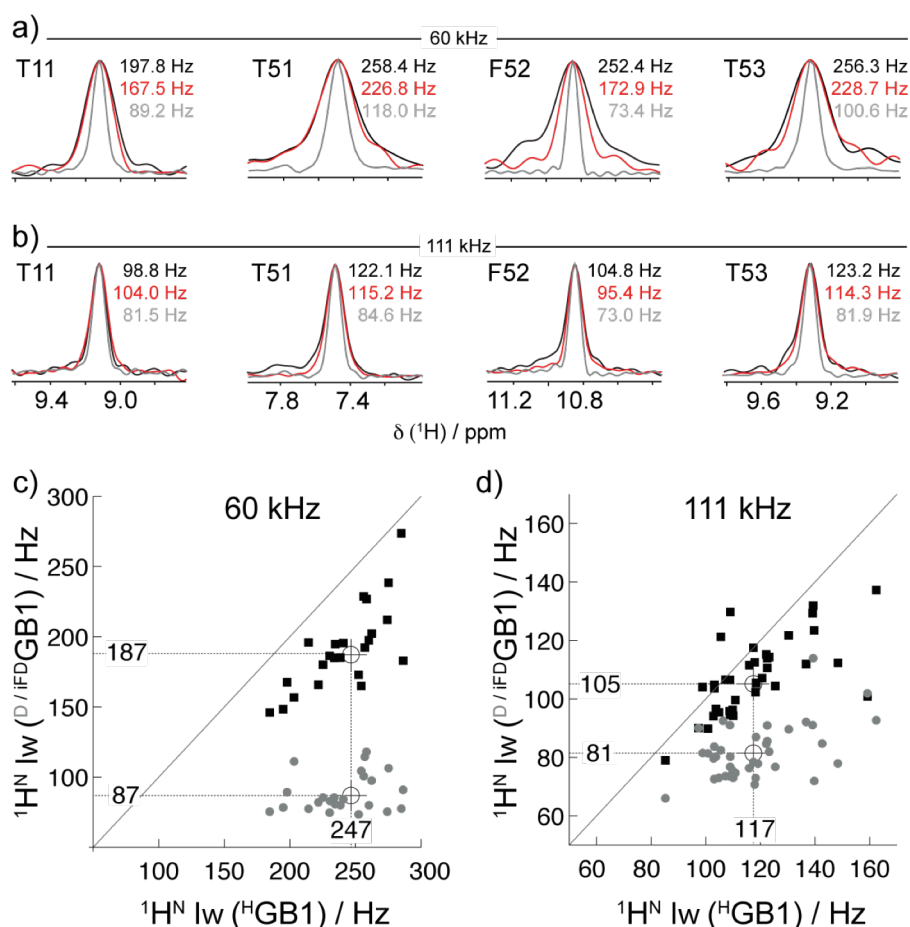**Fig. 2.** ^{1}H cross-sections from the ^{15}N-CP-HSQC of ^{D}GB1 (grey), ^{iFD}GB1 (red) and ^{H}GB1 (black), recorded with 60 kHz (a) and 111 kHz (b) MAS on a 1 GHz spectrometer, normalized w.r.t. peak intensity. Correlations between ^{1}H linewidths observed for resolved cross-signals in either ^{D}GB1 (grey circles) or ^{iFD}GB1 (black squares) and ^{H}GB1, at 60 kHz (c) and 111 kHz (d) MAS. The median of obtained values is shown by a crossed circle in each plot.

portion of the observed linewidths, indicating more balanced homogeneous and inhomogeneous contributions. Median linewidths of amide and α-protons and their approximate homoneneous and inhomogenous contributions are summarized in Table 1. Contrary to ^{1}H linewidths, the feasibility of recording INEPT-HSQC spectra is determined solely by the ^{1}H coherence lifetime. Such spectra are of particular interest for example for samples with extended flexible regions [48], but yet inaccessible without extensive deuteration. In Figure 6 we compare the relative efficiency of dipolar- and scalar-based ^{15}N-^{1}H correlation spectra for the three GB1 samples discussed above. Thanks to the long ^{1}H^N coherence lifetime at 111 kHz MAS, the integral signal in the INEPT-HSQC is 76% w.r.t. the CP-HSQC for ^{D}GB1. In ^{iFD}GB1 and ^{H}GB1, however, the respective ratio is about 25-30%. In these conditions it is feasible to acquire a complete 2D correlation within 1 hour (Fig. 6d,e), however, significantly longer acquisition is required for samples with less intrinsic sensitivity or shorter ^{1}H coherence lifetime. Further benefits in resolution and sensitivity of scalar-based correlations are therefore anticipated with the advent of a new generation of probes with capability for faster MAS.

Coherence lifetimes were also measured for ^{15}N, ^{13}Cα and ^{13}C' under low power ^{1}H decoupling and summarized in Figure 5. Due to proximity to proton(s), ^{13}Cα and ^{15}N show the largest T_2' enhancement (>100%) when MAS rate is increased from 60 to 111 kHz for all samples, and smaller but relevant gains (up to 80%) are observed for ^{13}C' (except for ^{D}GB1). Longer T_2' are connected to higher efficiencies of scalar-based ^{13}C-^{13}C coherence transfers,

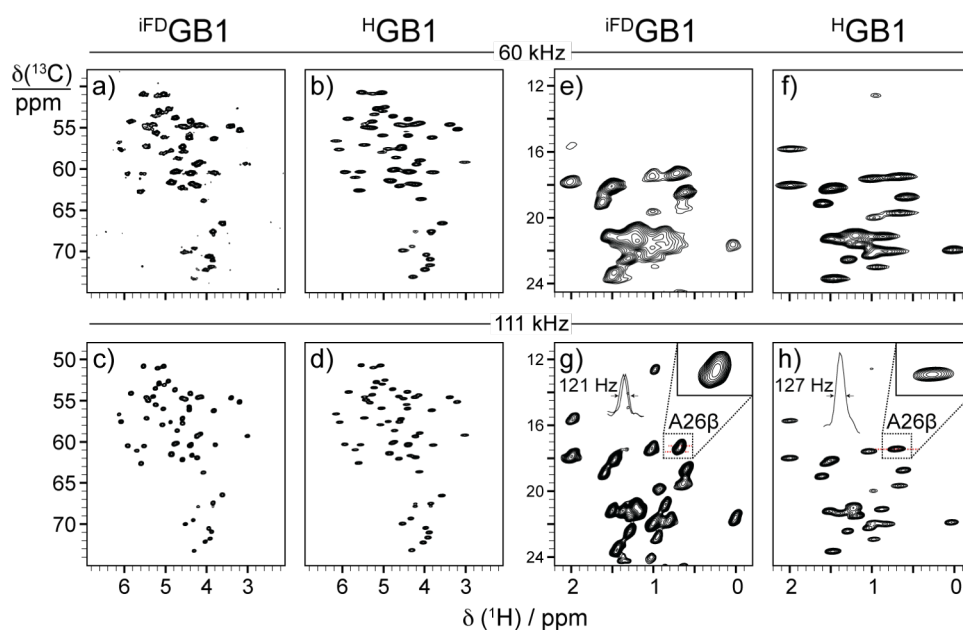**Fig. 3.** Hα-Cα (a-d) and methyl regions (e-h) of ^{13}C-CP-HSQC of [iFD]GB1 (a,c,e,g) and [H]GB1 (b,d,f,h) recorded on a 1 GHz spectrometer with 60 kHz (a,b,e,f) and 111 kHz (c,d,g,h) MAS. Representative ^{1}H cross-sections and linewidths are reported for the Cβ-Hβ correlation of Ala26 (g,h). In order to faithfully reproduce the linewidths in 2D contour plots, the lowest contour was normalized for each spectrum with respect to an average intensity of five resolved peaks (E15, T17, V21, V29, T51). The ratio of contour levels was set to 1.2.

which are essential building blocks of triple-resonance experiments. The sensitivity of experiments such as (H)(CA)CB(CA)NH or (H)(CO)CA(CO)NH [49] is therefore enhanced at faster MAS.

It is worth noting that inverse fractional deuteration extends all heteronuclear T_2' by approximately 50% w.r.t. full protonation. Despite this, full protonation at faster MAS yields higher ^{13}C resolution. In fact, inverse fractional deuteration entails random incorporation of deuterons in the side-chains, inevitably leading to mixtures of isotopomers. As a consequence of the [2]H-induced ^{13}C isotope shift and additional [1]J_{CD} couplings, side-chain ^{13}C resolution is deteriorated for a number of specific residues in [iFD]GB1. As shown in Figure 3e-h, this adverse effect is pronounced for methyl groups of alanines, valines, leucines and γ_2-site of isoleucines, where the populations of isotopomers are similar (CH_3:CH_2D:CHD_2 ratio is 1:3:3, assuming 50% random deuteration). Interestingly, for [iFD]GB1 methyl signals also exhibit a non-negligible [2]H-induced ^{1}H isotope shift, which confers a skewed appearance to the 2D lineshapes, and overall offsets any resolution advantage associated to the ^{1}H dilution. In contrast, for these signals fast MAS on a fully protonated sample combines full ^{1}H occupancy with optimal ^{13}C resolution. In the case of [13]Cα-Hα correlations for [iFD]GB1, we do not observe any loss of sensitivity since α-protons are recruited from the protonated solvent (less than 5% of [1]Hα dilution as quantified by Medeiros-Silva [39]), and linewidths are slightly improved compared to [H]GB1. In contrast, a significant deuteration level for most methyl and certain methylene groups (up to 50%), combined with adverse isotope effects, overall leads to a substantial loss of sensitivity w.r.t. a fully protonated sample at 111 kHz MAS. Unfortunately, a reliable quantification of S/N ratio of resonances in [13]C-^{1}H correlation spectra is impeded by variability of the actual amount of protein in 0.7 mm rotors.
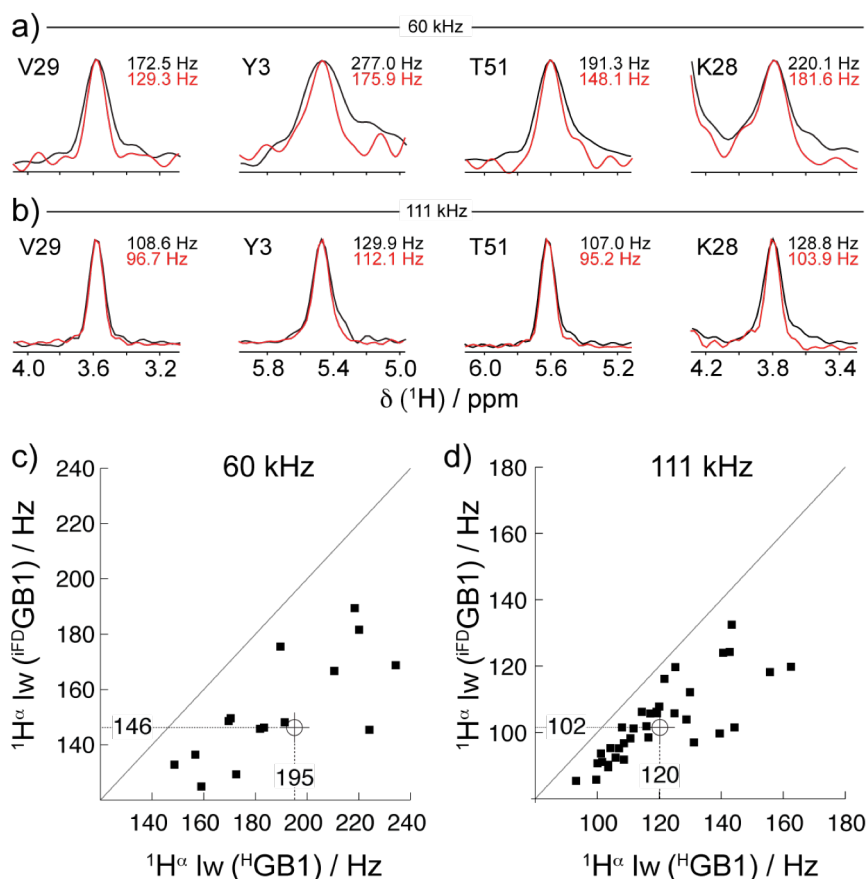
Fig. 4. $^1H\alpha$ cross-sections extracted from the ^{13}C-CP-HSQC of ^{iFD}GB1 (red) and ^{H}GB1 (black) recorded on a 1 GHz spectrometer with MAS rates of 60 kHz (a) and 111 kHz (b), normalized w.r.t. peak intensity. Correlations between $^1H\alpha$ linewidths observed for resolved cross-signals in ^{iFD}GB1 and ^{H}GB1, at MAS rates of 60 kHz (c) and 111 kHz (d). The median of the values of each plot is denoted by a crossed circle.

Aromatic ^{1}H side-chain resonances are relevant yet under-explored NMR probes in solid-state NMR. Here fast MAS delivers aromatic ^{13}C-CP-HSQC fingerprints with unprecedented quality (Fig. 7). As shown for ^{H}GB1, signals from all aromatic residues (1 Tryptophane, 3 Tyrosine and 2 Phenylalanine) are detectable with ^{1}H linewidths varying from 105 to 185 Hz. Notably, the spectral pattern of ^{iFD}GB1 is affected by uneven incorporation of deuterons into aromatic rings (Fig. 7a). Specifically, the Hζ_3 resonance of Trp vanishes upon iFD and intensity of Hδ_1 is significantly reduced. In contrast, the intensities of Hϵ_3, Hϵ_2 and Hζ_2 remain largely unaffected, although Hϵ_3 experiences almost 30% decrease in ^{1}H linewidth, as expected from deuteration at Hζ_3 position. Tyr Hϵ are present with full intensity in ^{iFD}GB1, while significant ^{1}H-dilution is observed for δ-protons. Finally, population of all protons in Phe rings is greatly decreased, the effect being difficult to quantify due to signal overlap between δ, ε and ζ protons. Overall, the dilution of aromatic protons improves ^{1}H linewidths for some aromatic and proximal aliphatic protons, but at the same time it removes structurally relevant NMR probes.

Table 1. Summary of linewidths for amide and α-protons for different preparations of GB1 and AP205.

Sample	MAS rate (kHz)	$^1\text{H}^\text{N}$ lw$_\text{exp}$[a] (Hz)	$^1\text{H}^\text{N}$ lw$_\text{hom}$[b] / lw$_\text{inh}$[c] (Hz)	$^1\text{H}^\alpha$ lw$_\text{exp}$[a] (Hz)
$^\text{H}$GB1	60	247±34	182 / 73	195±47
	111	117±21	59 / 73	120±21
$^\text{iFD}$GB1	60	187±32	132 / 73	146±19
	111	105±14	46 / 73	102±12
$^\text{D}$GB1	60	87±14	25 / 73	n/a
	111	81±13	14[d] / 73	n/a
$^\text{H}$AP205	111	139±31	106[d] / –[e]	119±31
$^\text{iFD}$AP205	111	112±17	96[d] / –[e]	99±30

[a] median and standard deviation of residue-specific linewidths (FWHH)

[b] median of homogeneous contribution to linewidth estimated for each residue. In absence of residue-specific T_2' data, we assumed a Voigt line shape with effective linewidth (lw$_\text{exp}$) dependent on Lorentzian homogeneous broadening (lw$_\text{hom}$) and Gaussian inhomogeneous broadening (lw$_\text{inh}$) according to the approximate formula: lw$_\text{exp}$ = 0.5346 lw$_\text{hom}$ + (0.2166 lw$_\text{hom}^2$ +lw$_\text{inh}^2$)$^{1/2}$

[c] median of inhomogeneous contribution to linewidth. It was assumed that inhomogeneity was uniform between samples, and lw$_\text{inh}$ equal to value for the respective residue in $^\text{D}$GB1 at 111 kHz MAS

[d] homogeneous contribution estimated from the bulk T_2' measurement as $1/(\pi T_2')$, and assumed equal for all residues in $^\text{D}$GB1

[e] contributions to linewidths not evaluated in absence of reference data for deuterated AP205 sample

It is noteworthy that the overall benefit of inverse fractional deuteration depends on the amino acid composition of a protein. Figure 8 shows an approximate level of deuteration at particular positions of aliphatic side-chains, based on analysis of amino acid synthetic pathways in bacteria as well as experimental data reported by Medeiros-Silva et al [39]. When expression is performed in 100% H_2O, most deuterons present in ^{2}H-enriched glucose are transferred to the solvent, and only specific positions of 8 amino acid types remain deuterated to more than 30%. In particular, the primary sequence of GB1 is devoid of serines, the amino acid with the highest incorporation of deuterons. Therefore, to draw more general conclusions we prepared an iFD sample of *Acinetobacter phage* 205 coat protein (130 a.a.), assembled in 2.5 MDa virus-like particles of 180 near-equivalent copies [50, 51]. The frequency of the 8 amino acids with high incorporation level of deuterons (S, A, E, Q, P, V, L, I) for AP205 is considerably higher (55% of the sequence) than for GB1 (38%); in particular, serines comprise 10% of the AP205CP sequence. The fingerprint spectra were acquired under the same experimental conditions as used in a study of the fully protonated AP205CP [36]. The ^{15}N-CP-HSQC and the α-regions of the ^{13}C-CP-HSQC spectra are shown in Figure 9a-b. Considerably higher spectral overlap is seen than for GB1, thus only 12 and 18 well resolved and intense peaks in each spectrum were selected for reliable linewidth estimation. Representative ^{1}H cross-sections from these spectra for both $^\text{iFD}$AP205 and $^\text{H}$AP205 are shown in Figure 9e-f, and the entire linewidth statistics compared in Figure 9c-d. In the case of AP205, iFD provides statistically meaningful decrease of linewidths even at 100 kHz MAS, with approximately the same relative effect on amide (-19%) and alpha (-17%) protons. The benefits of iFD are thus more emphasized than for GB1, which could be explained by (i) higher deuteration content and (ii) an overall higher relative contribution of homogeneous broadening to the linewidths. For example, bulk $^1\text{H}^\text{N}$ coherence lifetimes at 100 kHz MAS are 3.3 and 3.0 ms for $^\text{iFD}$AP205 and $^\text{H}$AP205 samples, which corresponds to homogeneous linewidths of 96 and 106 Hz, respectively. These linewidths are significantly larger than for GB1, and are likely to be more representative of samples that are intrinsically more flexible or non-crystalline [46]. Coherent effects thus still determine the ^{1}H resolution at 100 kHz MAS of either the fully protonated or iFD sample, and further linewidth reduction is envisaged with faster MAS.

3. Conclusions

We showed that the increase of MAS rates from 60 to 100 kHz (or 111 kHz) at ultra-high field provides a significantly higher improvement in resolution for ^{1}H resonances than what could be achieved by fractional deuteration. Both approaches may be jointly applied to improve resolution of amide or α-protons, however, linewidths are still inferior to the case of perdeuteration with 100% amide ^{1}H^N back-exchange. Even at 111 kHz MAS, we observed a strong dependence of ^{1}H and heteronuclear coherence lifetimes on the deuteration level. For these two reasons, either highly or fractionally deuterated samples facilitate sequence-specific backbone resonance assignment. However, fully protonated proteins show higher resolution and sensitivity in aliphatic side-chains, and specifically for methyl resonances. Resolution benefits of the iFD labeling scheme seem to be quite dependent on the amino acid composition of a protein. We conclude that fully protonated samples represent a more general and versatile solution for studies at ultrafast MAS.

Materials and Methods
Sample preparation

Uniformly ^{13}C,^{15}N-labeled GB1 and AP205 coat protein (AP205CP) samples were expressed in *Escherichia coli*, purified, and crystallized as described previously [36, 51-53]. To obtain samples with different proton/deuterium ratio, ^{iFD}GB1 and ^{iFD}AP205CP were expressed in H_2O-based medium containing 1.0 g/L of ^{15}NH$_4$Cl and 2 g/L of *deuterated* ^{13}C-glucose (d7) [39], while ^{H}GB1 and ^{H}AP205CP were expressed using H_2O and *protonated* ^{13}C-glucose. ^{D}GB1 was expressed using D_2O-based medium containing ^{15}NH$_4$Cl and deuterated ^{13}C-glucose, lyophilized two times from D_2O before addition in the medium. All the proteins were then extracted, purified and microcrystallized in H_2O-based buffer according to the protocols described previously. Microcrystals were harvested and packed into 0.7 mm rotors by ultracentrifugation at 120,000 ×g at 4°C for 1 hour using a 1.3 mm device purchased from Giotto Biotech [54, 55]. A 0.7 mm rotor was inserted into a 1.3 mm rotor and sealed with two fluorinated rubber plugs at the bottom side of the larger rotor. The packing protocol is under constant development and readers are encouraged to contact the authors for up-to-date advice.

NMR spectroscopy and data processing

All spectra were acquired on a 1 GHz spectrometer and MAS rate of 60 kHz (AP205CP and GB1), 100 kHz (AP205CP) or 111 kHz (GB1) using a Bruker 0.7 mm HCN probe. Sample temperature was
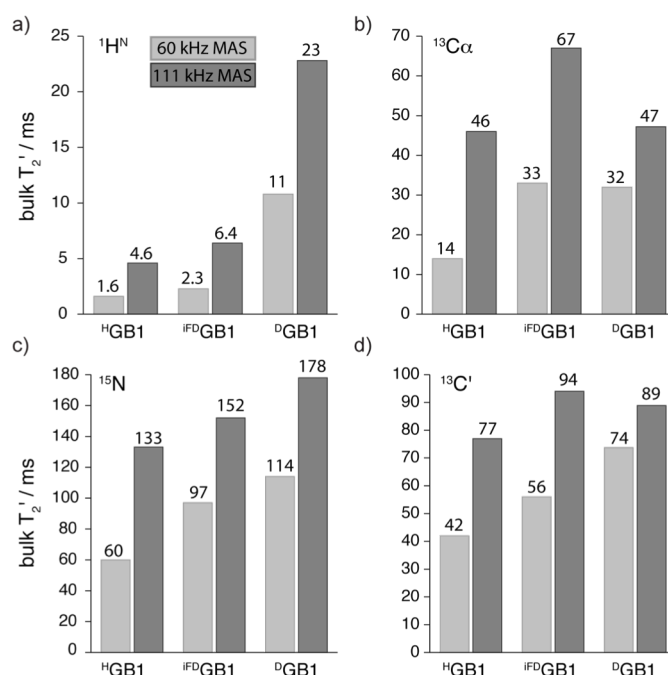

Fig. 5. Bulk transverse coherence lifetimes (T$_2$') of ^{1}H^N (a), ^{13}Cα (b), ^{15}N (c) and ^{13}C' (d) measured for GB1 samples on a 1 GHz spectrometer at 60 (*grey* bars) and 111 kHz (*black* bars) MAS under low power heteronuclear ^{1}H decoupling for ^{13}C and ^{15}N (see *Materials and Methods*).

maintained at about 10°C using a Bruker cooling unit with regulated N_2 gas directed at the rotor. The temperature of this gas measured just before reaching the sample was 280, 260 and 255 K at 60, 100 and 111 kHz MAS respectively. The rotor with [iFD]AP205 was spun only to 100 kHz without exceeding a limit of 5 bar drive pressure in the prototype 0.7 mm probe (note that since then the stator has been redesigned).

The dipolar-based ^{15}N- and ^{13}C-HSQC experiments follow, with little modifications, those introduced by Rienstra and co-workers [40, 56]. For ^1H-^{15}N and ^1H-^{13}C CP, we optimized around nutation frequencies of $5/4\ \omega_R$ for ^1H and $1/4\ \omega_R$ for heteronuclei (^{15}N or ^{13}C), with a 10% linear ramp applied on the ^1H channel. Low-power WALTZ-16 proton decoupling of 10 kHz was applied for heteronuclear decoupling for [D]GB1 and [iFD]GB1 samples, whereas for [H]GB1 low-power slTPPM of 15 and 27 kHz was applied at 60 and 111 kHz MAS, respectively [57]. The optimal decoupling scheme was chosen for each sample to obtain maximum $^{15}N\ T_2'$. Note that at 111 kHz MAS slTPPM decoupling with 10-15 kHz ^1H RF may perform better than with 27 kHz RF. Suppression of solvent signals [8] was achieved using the MISSISSIPPI scheme [58] applied for 200 ms, and the interscan delay ranged from 0.8 to 1 s for GB1, and 1–1.4 s for AP205CP.

Concerning coherence lifetimes, ^{15}N and ^1H bulk coherence lifetimes (T_2') were measured using a ^{15}N-CP-HSQC pulse sequence with a variable-time echo period on the respective channel. For $^{13}C\ T_2'$,
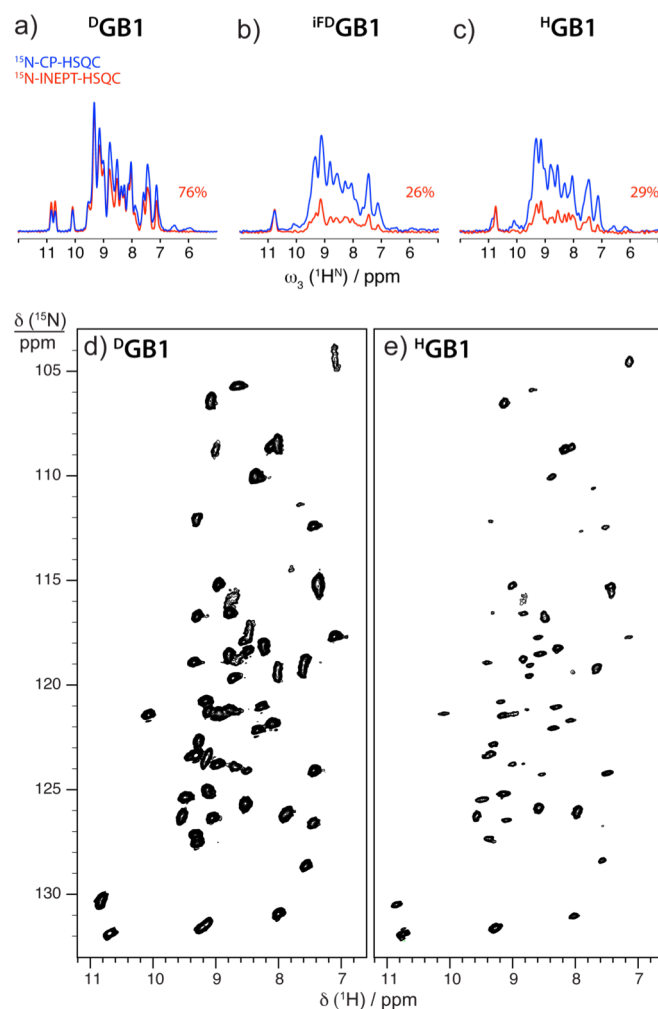

Fig. 6. Relative efficiency of dipolar- (in blue) and scalar-based (in red) HSQC shown on 1D first-FID spectra for [D]GB1 (a), [iFD]GB1 (b) and [H]GB1 (c). CP-HSQC spectra were normalized between samples to show equal integrals (a-c). Relative scale of CP- and INEPT-HSQC was preserved, and the ratio of their integrals is reported on every panel. 2D ^{15}N-INEPT-HSQC spectra for [D]GB1 (d) and [H]GB1 (e) acquired in the same experimental time of 1 hour at 111 kHz MAS and at 1 GHz spectrometer. To reflect the difference in sensitivity, spectra are plotted with the same contour scale with the lowest contour at 5 standard deviations of noise, and the ratio between contours of 1.2.
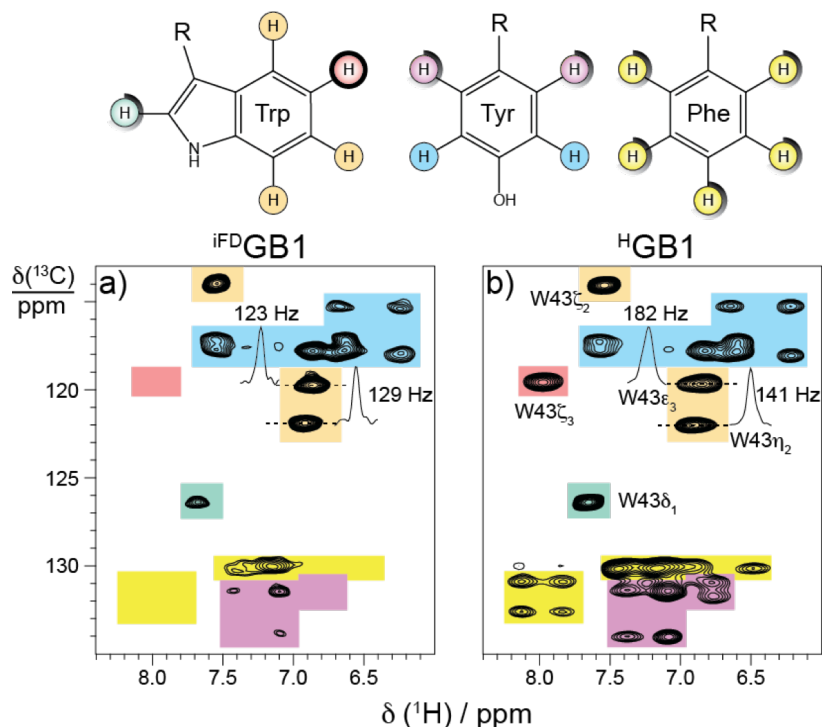
Fig. 7. Aromatic region of ^{13}C-CP-HSQC of [iFD]GB1 (a) and [H]GB1 (b) recorded on a 1 GHz spectrometer with 111 kHz MAS. [1]H cross-sections and linewidths are reported for two signals of Trp43. A color code illustrates the amino acid-specific assignments of tryptophan, tyrosine and phenylalanine protons, while a black ring of increasing angular width reports on the approximate extent of suppression of a signal by deuteration (no impact, no circle; deletion, bold black circle). In order to faithfully reproduce the linewidths in 2D contour plots, the lowest contour was normalized for each spectrum with respect to an average intensity of two resolved W43 peaks (ζ_2 and η_2). The ratio of contour levels was set to 1.2.

we employed a carbon-detected CP sequence with a selective refocusing pulse. ReBURP [59] pulses of duration of 680 ms and 1300 ms were applied for [13]C' and [13]Cα, at the ^{13}C carrier offsets of 176 and 58 ppm, respectively.

Spectra were apodized in the indirect dimension with 60° shifted square sine-bells (« qsine 3 » in Bruker Topspin), and zero-filled to at least four times the number of points in all dimensions. No apodization was applied in ^{1}H dimension. [1]H FID signals were truncated to 15 ms, which ensures a minimal impact on measured linewidths. All spectra were analyzed using NMRFAM-Sparky [60]. Linewidths were estimated using a built-in utility, and report on full width at half-height of peaks centered at the maximum intensity. No peak fitting nor integration was applied due to common deviation from a Lorentzian shape.

Shimming, magnet stability and magic-angle adjustment
Probe shimming was performed using a sample of adamantane, where about 5 Hz linewidth was achieved in the ^{13}C spectrum. Independently, field homogeneity was verified to be less than 20 Hz using a residual ^{1}H methyl resonance in a rotor filled with a liquid [2]H-methanol (CD$_3$OD). This was repeated before a series of measurements for every protein sample.

Magic-angle was verified or adjusted at every MAS rate after stabilization of conditions (rotation rate and temperature) to ensure maximum [1]H^N coherence lifetime and thus optimal resolution in ^{1}H dimension. This was monitored as intensity of 1D ^{1}H spectrum acquired with ^{15}N-CP-HSQC pulse sequence with an appended ^{1}H echo of a fixed duration of approximately T$_2$'.

Data were acquired without the use of a lock. The impact of B$_0$ field stability during experiments was monitored using 1D ^{1}H spectra, and, due to short total acquisition time, has negligible effect on resolution of acquired 2D spectra (less than 10 Hz drift).
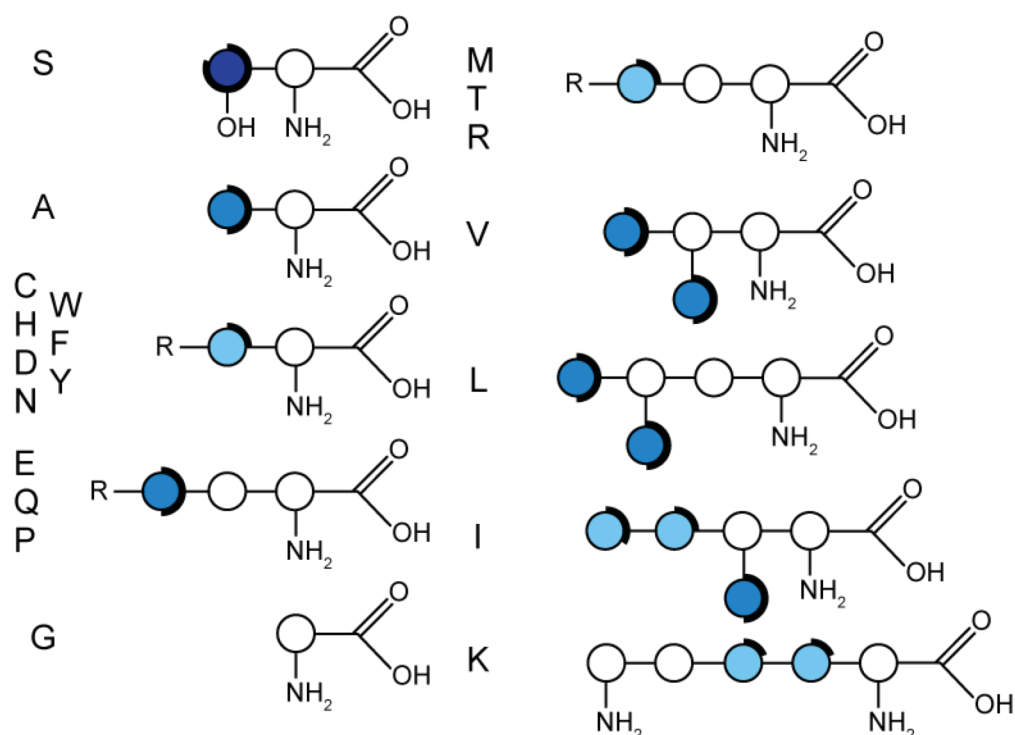
Fig. 8. Schematic representation of ^{1}H dilution by inverse fractional deuteration, based on biosynthetic pathway analysis and experimental data on expression in *E. coli* BL21(DE3) cells reported by Medeiros-Silva et al. [39]. The degree of ^{2}H incorporation is illustrated by black rings of growing angular width and blue circles of increasing intensity: 0 to 10% (white), 11 to 30% (light blue), 31 to 50% (medium blue), more than 51% (dark blue).
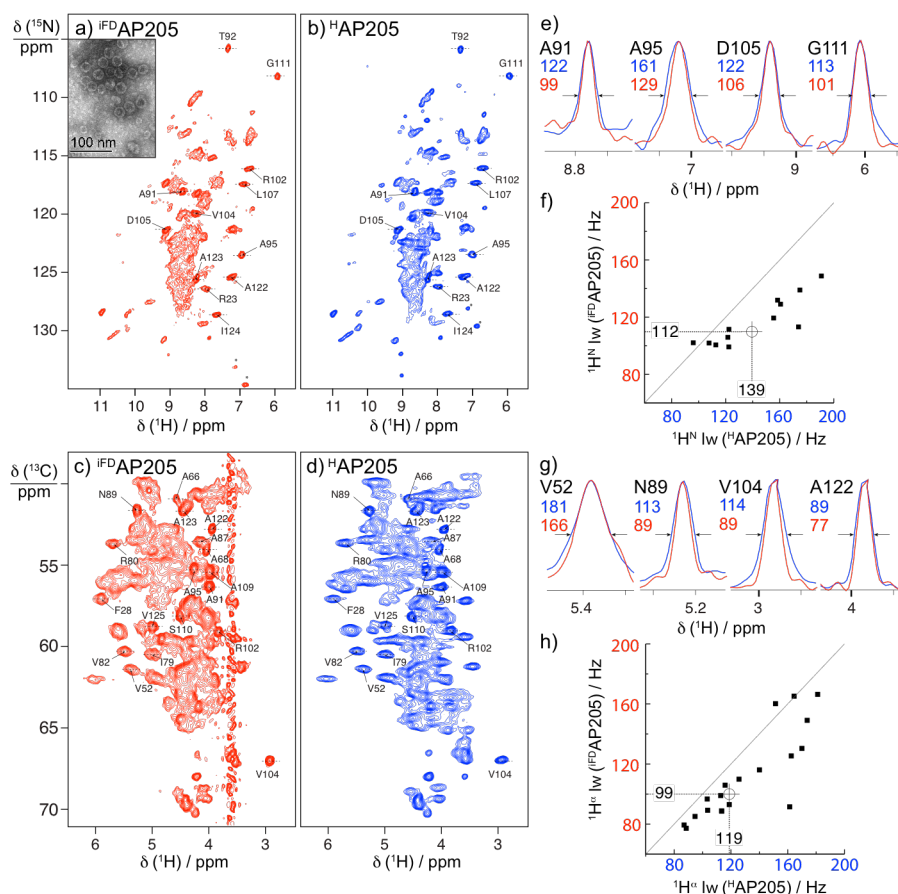
Fig. 9. ^{15}N-CP-HSQC (a,b) and α-region of the ^{13}C-CP-HSQC (c,d) of AP205 coat protein recorded on a 1 GHz spectrometer and 100 kHz MAS. Compared are the spectra of [iFD]AP205 (a,c; *red* contours) and [H]AP205 (b, d; *blue* contours). 12 and 18 isolated intense resonances for which ^{1}H linewidths were evaluated are labeled in (a-d). Representative ^{1}H cross-sections from ^{15}N- (e) or ^{13}C-CP-HSQC (g). Linewidths for fully-protonated (in *blue*) and iFD samples (in *red*) are indicated below residue names (in Hertz). Comparison of [1]H[N] (f) and [1]Hα (h) linewidths between fully protonated and iFD samples. The median of linewidths is denoted by a crossed open circle and reported next to the respective axis. The contour levels are increasing exponentially with a multiplier of 1.2, and the lowest contour was normalized between spectra (a and b; c and d) with respect to the average intensity of all isolated peaks to properly reflect linewidths.

References

[1] G. Bodenhausen, D.J. Ruben, Natural abundance nitrogen-15 NMR by enhanced heteronuclear spectroscopy, Chem. Phys. Lett. 69 (1980) 185-189.

[2] Y. Ishii, J.P. Yesinowski, R. Tycko, Sensitivity Enhancement in Solid-State 13C NMR of Synthetic Polymers and Biopolymers by 1H NMR Detection with High-Speed Magic Angle Spinning, J. Am. Chem. Soc. 123 (2001) 2921-2922.

[3] M.M. Maricq, J.S. Waugh, NMR in rotating solids, J. Chem. Phys. 70 (1979) 3300-3316.

[4] A.E. McDermott, F.J. Creuzet, A.C. Kolbert, R.G. Griffin, High-resolution magic-angle-spinning NMR spectra of protons in deuterated solids, J. Magn. Reson. 98 (1992) 408-413.

[5] L. Zheng, K.W. Fishbein, R.G. Griffin, J. Herzfeld, Two-dimensional solid-state proton NMR and proton exchange, J. Am. Chem. Soc. 115 (1993) 6254-6261.

[6] B. Reif, C.P. Jaroniec, C.M. Rienstra, M. Hohwy, R.G. Griffin, 1H-1H MAS correlation spectroscopy and distance measurements in a deuterated peptide, J. Magn. Reson. 151 (2001) 320-327.

[7] V. Chevelkov, B.J. van Rossum, F. Castellani, K. Rehbein, A. Diehl, M. Hohwy, S. Steuernagel, F. Engelke, H. Oschkinat, B. Reif, 1H detection in MAS solid-state NMR spectroscopy of biomacromolecules employing pulsed field gradients for residual solvent suppression, J. Am. Chem. Soc. 125 (2003) 7788-7789.

[8] E.K. Paulson, C.R. Morcombe, V. Gaponenko, B. Dancheck, R.A. Byrd, K.W. Zilm, Sensitive high resolution inverse detection NMR spectroscopy of proteins in the solid state, J. Am. Chem. Soc. 125 (2003) 15831-15836.

[9] V. Chevelkov, K. Rehbein, A. Diehl, B. Reif, Ultrahigh resolution in proton solid-state NMR spectroscopy at high levels of deuteration, Angew. Chem. Int. Ed. Engl. 45 (2006) 3878-3881.

[10] D.H. Zhou, D.T. Graesser, W.T. Franks, C.M. Rienstra, Sensitivity and resolution in proton solid-state NMR at intermediate deuteration levels: Quantitative linewidth characterization and applications to correlation spectroscopy, J. Magn. Reson. 178 (2006) 297-307.

[11] Ü. Akbey, S. Lange, W.T. Franks, R. Linser, K. Rehbein, A. Diehl, B.-J. van Rossum, B. Reif, H. Oschkinat, Optimum Levels of Exchangeable Protons in Perdeuterated Proteins for Proton Detection in MAS Solid-State NMR Spectroscopy, J. Biomol. NMR 46 (2010) 67–73.

[12] A. Samoson, T. Tuherm, Z. Gan, High-field high-speed MAS resolution enhancement in 1H NMR spectroscopy of solids, Solid State Nucl Magn Reson 20 (2001) 130-6.

[13] L.B. Andreas, T. Le Marchand, K. Jaudzems, G. Pintacuda, High-resolution proton-detected NMR of proteins at very fast MAS, J. Magn. Reson. 253 (2015) 36-49.

[14] A. Böckmann, M. Ernst, B.H. Meier, Spinning proteins, the faster, the better?, J. Magn. Reson. 253 (2015) 71-79.

[15] J.R. Lewandowski, J.N. Dumez, Ü. Akbey, S. Lange, L. Emsley, H. Oschkinat, Enhanced resolution and coherence lifetimes in the solid-state NMR spectroscopy of perdeuterated proteins under ultrafast Magic-Angle Spinning, J. Chem. Phys. Lett. 2 (2011) 2205-2211.

[16] M.J. Knight, A.L. Webber, A.J. Pell, P. Guerry, E. Barbet-Massin, I. Bertini, I.C. Felli, L. Gonnelli, R. Pierattelli, L. Emsley, A. Lesage, T. Herrmann, G. Pintacuda, Fast resonance assignment and fold determination of human superoxide dismutase by high-resolution proton-detected solid-state MAS NMR spectroscopy, Angew. Chem. Int. Ed. Engl. 50 (2011) 11697-11701.

[17] A.J. Nieuwkoop, W.T. Franks, K. Rehbein, A. Diehl, Ü. Akbey, F. Engelke, L. Emsley, G. Pintacuda, H. Oschkinat, Sensitivity and resolution of proton detected spectra of a deuterated protein at 40 and 60 kHz magic-angle-spinning, J. Biomol. NMR 61 (2015) 161-171.

[18] V. Agarwal, S. Penzel, K. Szekely, R. Cadalbert, E. Testori, A. Oss, J. Past, A. Samoson, M. Ernst, A. Böckmann, B.H. Meier, De Novo 3D Structure Determination from Sub-milligram Protein Samples by Solid-State 100 kHz MAS NMR Spectroscopy, Angew. Chem. Int. Ed. 53 (2014) 12253-12256.

[19] J.M. Lamley, D. Iuga, C. Öster, H.-J. Sass, M. Rogowski, A. Oss, J. Past, A. Reinhold, S. Grzesiek, A. Samoson, J.R. Lewandowski, Solid-State NMR of a Protein in a Precipitated Complex with a Full-Length Antibody, J. Am. Chem. Soc. 136 (2014) 16800-16806.

[20] L.B. Andreas, J. Stanek, T. Le Marchand, A. Bertarello, D. Cala-De Paepe, D. Lalli, M. Krejčíková, C. Doyen, C. Öster, B. Knott, S. Wegner, F. Engelke, I.C. Felli, R. Pierattelli, N.E. Dixon, L. Emsley, T. Herrmann, G. Pintacuda, Protein residue linking in a single spectrum for magic-angle spinning NMR assignment, J. Biomol. NMR 62 (2015) 253-61.

[21] V. Agarwal, B. Reif, Residual methyl protonation in perdeuterated proteins for multi-dimensional correlation experiments in MAS solid-state NMR spectroscopy, J. Magn. Reson. 194 (2008) 16-24.

[22] V. Agarwal, A. Diehl, N. Skrynnikov, B. Reif, High resolution 1H detected 1H,13C correlation spectra in MAS solid-state NMR using deuterated proteins with selective 1H,2H isotopic labeling of methyl groups, J. Am. Chem. Soc. 128 (2006) 12620-12621.

[23] S. Asami, P. Schmieder, B. Reif, High resolution 1H-detected solid-state NMR spectroscopy of protein aliphatic resonances: access to tertiary structure information, J. Am. Chem. Soc. 132 (2010) 15133-15135.

[24] S. Asami, K. Szekely, P. Schanda, B.H. Meier, B. Reif, Optimal degree of protonation for (1)H detection of aliphatic sites in randomly deuterated proteins as a function of the MAS frequency, J. Biomol. NMR 54 (2012) 155-168.

[25] D. Mance, T. Sinnige, M. Kaplan, S. Narasimhan, M. Daniels, K. Houben, M. Baldus, M. Weingarth, An Efficient Labelling Approach to Harness Backbone and Side-Chain Protons in (1)H-Detected Solid-State NMR Spectroscopy, Angew. Chem. Int. Ed. Engl. 54 (2015) 15799-15803.

[26] K.H. Gardner, M.K. Rosen, L.E. Kay, Global folds of highly deuterated, methyl-protonated proteins by multidimensional NMR, Biochemistry 36 (1997) 1389-1401.

[27] N.K. Goto, K.H. Gardner, G.A. Mueller, R.C. Willis, L.E. Kay, A robust and cost-effective method for the production of Val, Leu, Ile (delta 1) methyl-protonated 15N-, 13C-, 2H-labeled proteins, J. Biomol. NMR 13 (1999) 369-374.

[28] P. Gans, O. Hamelin, R. Sounier, I. Ayala, M.A. Dura, C.D. Amero, M. Noirclerc-Savoye, B. Franzetti, M.J. Plevin, J. Boisbouvier, Stereospecific isotopic labeling of methyl groups for NMR

spectroscopic studies of high-molecular-weight proteins, Angew. Chem. Int. Ed. Engl. 49 (2010) 1958-1962.

[29] M. Huber, S. Hiller, P. Schanda, M. Ernst, A. Böckmann, R. Verel, B.H. Meier, A proton-detected 4D solid-state NMR experiment for protein structure determination, ChemPhysChem 12 (2011) 915-918.

[30] V. Kurauskas, E. Crublet, P. Macek, R. Kerfah, D.F. Gauto, J. Boisbouvier, P. Schanda, Sensitive proton-detected solid-state NMR spectroscopy of large proteins with selective CH3 labelling: application to the 50S ribosome subunit, Chem. Commun. 52 (2016) 9558-9561.

[31] R. Linser, B. Bardiaux, V. Higman, U. Fink, B. Reif, Structure calculation from unambiguous long-range amide and methyl 1H-1H distance restraints for a microcrystalline protein with MAS solid-state NMR spectroscopy, J. Am. Chem. Soc. 133 (2011) 5905-5912.

[32] M. Kainosho, T. Torizawa, Y. Iwashita, T. Terauchi, A. Mei Ono, P. Güntert, Optimal isotope labelling for NMR protein structure determinations, Nature 440 (2006) 52-57.

[33] H. Takahashi, M. Kainosho, H. Akutsu, T. Fujiwara, 1H-detected 1H-1H correlation spectroscopy of a stereo-array isotope labeled amino acid under fast magic-angle spinning, J. Magn. Reson. 203 (2010) 253-256.

[34] S. Wang, S. Parthasarathy, Y. Nishiyama, Y. Endo, T. Nemoto, K. Yamauchi, T. Asakura, M. Takeda, T. Terauchi, M. Kainosho, Y. Ishii, Nano-mole scale side-chain signal assignment by 1H-detected protein solid-state NMR by ultra-fast magic-angle spinning and stereo-array isotope labeling, PLoS One 10 (2015) e0122714.

[35] T. Sinnige, M. Daniëls, M. Baldus, M. Weingarth, Proton Clouds to measure long-range contacts between nonexchangeable side chain protons in solid-state NMR, J. Am. Chem. Soc. 136 (2014) 4452-4455.

[36] L.B. Andreas, K. Jaudzems, J. Stanek, D. Lalli, A. Bertarello, T. Le Marchand, D. Cala-De Paepe, S. Kotelovica, I. Akopjana, B. Knott, S. Wegner, F. Engelke, A. Lesage, L. Emsley, K. Tars, T. Herrmann, G. Pintacuda, Structure of fully protonated proteins by proton-detected magic-angle spinning NMR, Proc. Natl. Acad. Sci. USA 113 (2016) 9187-9192.

[37] M.E. Ward, L. Shi, E. Lake, S. Krishnamurthy, H. Hutchins, L.S. Brown, V. Ladizhansky, Proton-detected solid-state NMR reveals intramembrane polar networks in a seven-helical transmembrane protein proteorhodopsin, J. Am. Chem. Soc. 133 (2011) 17434-17443.

[38] J.H. Chill, J.M. Louis, C. Miller, A. Bax, NMR study of the tetrameric KcsA potassium channel in detergent micelles, Protein Sci. 15 (2006) 684-698.

[39] J. Medeiros-Silva, D. Mance, M. Daniels, S. Jekhmane, K. Houben, M. Baldus, M. Weingarth, 1H-Detected Solid-State NMR Studies of Water-Inaccessible Proteins In Vitro and In Situ, Angew. Chem. Int. Ed. Engl. 55 (2016) 13606-13610.

[40] D.H. Zhou, G. Shah, M. Cormos, C. Mullen, D. Sandoz, C.M. Rienstra, Proton-detected solid-state NMR Spectroscopy of fully protonated proteins at 40 kHz magic-angle spinning, J. Am. Chem. Soc. 129 (2007) 11791-11801.

[41] A. Marchetti, S. Jehle, M. Felletti, M.J. Knight, Y. Wang, Z.Q. Xu, A.Y. Park, G. Otting, A. Lesage, L. Emsley, N.E. Dixon, G. Pintacuda, Backbone assignment of fully protonated solid proteins by 1H detection and ultrafast Magic-Angle-Spinning NMR spectroscopy, Angew. Chemie Int. Ed. Engl. 51 (2012) 10756-10759.

[42] S.K. Vasa, P. Rovo, K. Giller, S. Becker, R. Linser, Access to aliphatic protons as reporters in non-deuterated proteins by solid-state NMR, Phys. Chem. Chem. Phys. 18 (2016) 8359-8363.

[43] K.H. Mroue, Y. Nishiyama, M.K. Pandey, B. Gong, E. McNerny, D.H. Kohn, M.D. Morris, A. Ramamoorthy, Proton-Detected Solid-State NMR Spectroscopy of Bone with Ultrafast Magic Angle Spinning, Sci. Rep. 5 (2015) 11991.

[44] Y. Nishiyama, Fast magic-angle sample spinning solid-state NMR at 60-100kHz for natural abundance samples, Solid State Nucl. Magn. Reson. 78 (2016) 24-36.

[45] M.K. Pandey, Y. Nishiyama, Determination of NH proton chemical shift anisotropy with (14)N-(1)H heteronuclear decoupling using ultrafast magic angle spinning solid-state NMR, J. Magn. Reson. 261 (2015) 133-140.

[46] J. Stanek, L.B. Andreas, K. Jaudzems, D. Cala, D. Lalli, A. Bertarello, T. Schubeis, I. Akopjana, S. Kotelovica, K. Tars, A. Pica, S. Leone, D. Picone, Z.-Q. Xu, N.E. Dixon, D. Martinez, M. Berbon, N. El Mammeri, A. Noubhani, S. Saupe, B. Habenstein, A. Loquet, G. Pintacuda, NMR spectroscopic assignment of backbone and side‐chain protons in fully protonated proteins: microcrystals, sedimented assemblies, and amyloid fibrils, Angew. Chem. Int. Ed. 128 (2016) 15730-15735.

[47] H.L.F. Schmidt, L.J. Sperling, Y.G. Gao, B.J. Wylie, J.M. Boettcher, S.R. Wilson, C.M. Rienstra, Crystal polymorphism of protein GB1 examined by solid-state NMR spectroscopy and X-Ray diffraction, J. Phys. Chem. B 111 (2007) 14362-14369.

[48] H.R. Dannatt, M. Felletti, S. Jehle, Y. Wang, L. Emsley, N.E. Dixon, A. Lesage, G. Pintacuda, Weak and Transient Protein Interactions Determined by Solid-State NMR, Angew Chem Int Ed Engl 55 (2016) 6638-41.

[49] E. Barbet-Massin, A.J. Pell, K. Jaudzems, W.T. Franks, J.S. Retel, S. Kotelovica, I. Akopjana, K. Tars, L. Emsley, H. Oschkinat, A. Lesage, G. Pintacuda, Out-and-back 13C-13C scalar transfers in protein resonance assignment by proton-detected solid-state NMR under ultra-fast MAS, J. Biomol. NMR 56 (2013) 379-386.

[50] S.H. van den Worm, R.I. Koning, H.J. Warmenhoven, H.K. Koerten, J. van Duin, Cryo electron microscopy reconstructions of the Leviviridae unveil the densest icosahedral RNA packing possible, J. Mol. Biol. 363 (2006) 858-865.

[51] M. Shishovs, J. Rumnieks, C. Diebolder, K. Jaudzems, L.B. Andreas, J. Stanek, A. Kazaks, S. Kotelovica, I. Akopjana, G. Pintacuda, R.I. Koning, K. Tars, Structure of AP205 Coat Protein Reveals Circular Permutation in ssRNA Bacteriophages, J. Mol. Biol. 428 (2016) 4267-4279.

[52] E. Barbet-Massin, A.J. Pell, J.S. Retel, L.B. Andreas, K. Jaudzems, W.T. Franks, A.J. Nieuwkoop, M. Hiller, V. Higman, P. Guerry, A. Bertarello, M.J. Knight, M. Felletti, T. Le Marchand, S. Kotelovica, I. Akopjana, K. Tars, M. Stoppini, V. Bellotti, M. Bolognesi, S. Ricagno, J.J. Chou, R.G. Griffin, H. Oschkinat, A. Lesage, L. Emsley, T. Herrmann, G. Pintacuda, Rapid Proton-Detected NMR Assignment for Proteins with Fast Magic Angle Spinning, J. Am. Chem. Soc. 136 (2014) 12489-12497.

[53] W.T. Franks, D.H. Zhou, B.J. Wylie, B.G. Money, D.T. Graesser, H.L. Frericks, G. Sahota, C.M. Rienstra, Magic-angle spinning solid-state NMR spectroscopy of the β1 immunoglobulin binding domain of protein G (GB1): N-15 and C-13 chemical shift assignments and conformational analysis, J. Am. Chem. Soc. 127 (2005) 12291-12305.

[54] I. Bertini, F. Engelke, L. Gonnelli, B. Knott, C. Luchinat, D. Osen, E. Ravera, On the use of ultracentrifugal devices for sedimented solute NMR, J. Biomol. NMR 54 (2012) 123-127.

[55] C. Gardiennet, A.K. Schutz, A. Hunkeler, B. Kunert, L. Terradot, A. Böckmann, B.H. Meier, A sedimented sample of a 59 kDa dodecameric helicase yields high-resolution solid-state NMR spectra, Angew. Chem. Int. Ed. Engl. 51 (2012) 7855-7858.

[56] D.H. Zhou, J.J. Shea, A.J. Nieuwkoop, W.T. Franks, B.J. Wylie, C. Mullen, D. Sandoz, C.M. Rienstra, Solid-state protein-structure determination with proton-detected triple-resonance 3D magic-angle-spinning NMR spectroscopy, Angew. Chem. Int. Ed. Engl. 46 (2007) 8380-8383.

[57] J.R. Lewandowski, J. Sein, H.J. Sass, S. Grzesiek, M. Blackledge, L. Emsley, Measurement of site-specific 13C spin-lattice relaxation in a crystalline protein, J. Am. Chem. Soc. 132 (2010) 8252-8254.

[58] D.H. Zhou, C.M. Rienstra, High-performance solvent suppression for proton detected solid-state NMR, J. Magn. Reson. 192 (2008) 167-172.

[59] H. Geen, R. Freeman, Band-Selective Radiofrequency Pulses, J. Magn. Reson. 93 (1991) 93-141.

[60] W. Lee, M. Tonelli, J.L. Markley, NMRFAM-SPARKY: enhanced software for biomolecular NMR spectroscopy, Bioinformatics 31 (2015) 1325-1327.